In Vitro Cell.Dev.Biol.—Animal (2014) 50:129–138
DOI 10.1007/s11626-013-9684-3

Differential Effects of Hypoxic and Hyperoxic Stress-Induced Hypertrophy in Cultured Chick Fetal Cardiac Myocytes

Allison A. Greco · George Gomez

Received: 1 April 2013 / Accepted: 11 August 2013 / Published online: 29 August 2013 / Editor: T. Okamoto

Abstract The adult heart responds to contraction demands by hypertrophy, or enlargement, of cardiac myocytes. Adaptive hypertrophy can occur in response to hyperoxic conditions such as exercise, while pathological factors that result in hypoxia ultimately result in heart failure. The difference in the outcomes produced by pathologically versus physiologically induced hypertrophy suggests that the cellular signaling pathways or conditions of myocytes may be different at the cellular level. The structural and functional changes in myocytes resulting from hyperoxia (simulated using hydrogen peroxide) and hypoxia (using oxygen deprivation) were tested on fetal chick cardiac myocytes grown in vitro. Structural changes were measured using immunostaining for α-sarcomeric actin or MyoD, while functional changes were assessed using immunostaining for calcium/calmodulin-dependent kinase (CaMKII) and by measuring intracellular calcium fluxes using live cell fluorescence imaging. Both hypoxic and hyperoxic stress resulted in an upregulation of actin and MyoD expression. Similarly, voltage-gated channels governing myocyte depolarization and the regulation of CaMK were unchanged by hyperoxic or hypoxic conditions. However, the dynamic features of calcium fluxes elicited by caffeine or epinephrine were different in cells subjected to hypoxia versus hyperoxia, suggesting that these different conditions differentially affect components of ligand-activated signaling pathways that regulate calcium. Our results suggest that changes in signaling pathways, rather than structural organization, may mediate the different outcomes associated with hyperoxia-induced versus hypoxia-induced hypertrophy, and these changes are likely initiated at the cellular level.

Keywords Oxidative stress · Cardiac myocyte · Cell culture · Calcium fluxes · Chick heart

A. A. Greco · G. Gomez (✉)
Biology Department, University of Scranton, LSC 395,
204 Monroe Avenue, Scranton, PA 18510, USA
e-mail: george.gomez@scranton.edu

Present Address:
A. A. Greco
Thomas Jefferson University, Philadelphia, PA 19102, USA

Introduction

The heart is a dynamic organ that responds to short-term and long-term changes in the body. The adult heart responds to increased contraction demands with hypertrophy, or enlargement, of the cardiac myocytes themselves (Richey and Brown 1998; Frey and Olson 2003). This process can occur in response to physiological activities such as endurance exercise training, which produce adaptive muscle enlargement that results in increased oxygen delivery to body tissues (Moore and Korzick 1995). Pathologic conditions such as hypertension, diabetes, or heart disease can also result in cardiac muscle hypertrophy and are more likely to be associated with sudden death, the development of heart failure, and large myocardial infarctions due to ischemic death of heart tissue (Gaasch et al. 1990; Richey and Brown 1998). The difference in outcomes produced by pathologically versus physiologically induced hypertrophy suggests that the cellular signaling pathways or conditions of myocytes at the cellular level may be different (Kong et al. 2005). The goal of our study was to determine whether hypoxic and hyperoxic conditions differentially affected isolated cardiac myocyte growth properties.

Cardiac myocyte differentiation is marked by the production of specific isoforms of contractile fiber proteins (Sassoon et al. 1988; Aoki et al. 2000) that is regulated by the transcription factor MyoD (Olson 1993). The function of the contractile apparatus is supported by a number of different proteins and cellular mechanisms that involve the regulation of intracellular calcium (Maier and Bers 2007): calcium binds to

calcium/calmodulin-dependent kinase (CaMKII), which in turn phosphorylates the myosin regulatory light chain to activate myosin movement (Maier and Bers 2007). While we realize that there is a plethora of proteins involved with the structure and function of isolated myocytes, we focused our study on key proteins that are canonical marker molecules used to study cardiac myocytes: CaMKII (Zhang et al. 2003), MyoD (Chien et al. 1993), and α-sarcomeric actin (Waypa et al. 2002). We determined if the expression of these molecules was altered under conditions that promote hypertrophy.

Hypertrophic growth would also influence the functional properties of the cardiac myocytes. Since myocyte contraction is driven by the elevation of cytosolic calcium, we used calcium imaging to detect functional changes that could occur during cardiac muscle contraction as a result of hypertrophy. In an experimental setting, the depolarization of myocytes can be induced by bathing them in a solution containing high potassium concentrations (Berlin and Konishi 1993); depolarization releases calcium stored in the sarcoplasmic reticulum and activates CaMK, which facilitates myosin movement (Berlin and Konishi 1993). Pharmacological agents such as epinephrine bind to β-adrenergic receptors and initiate signaling cascades involving cyclic adenosine monophosphate activation of protein kinase A, which results in the activation of ryanodine receptors on the surface of the endoplasmic reticulum, causing the release of calcium from intracellular stores (Song et al. 2001). Similarly, caffeine stimulation triggers a depletion of sarcoplasmic reticulum Ca^{2+}, via the calcium-activated calcium release channels, resulting in prolonged Ca^{2+} elevation in the cytosol (Sitsapesan and Williams 1990; Bers 2000; Molkentin 2006). Thus, we quantified the calcium level changes occurring in cardiac myocytes as a result of stimulation by high potassium, epinephrine, or caffeine to study functional changes in the hypertrophic heart.

Fetal cardiac myocytes serve as useful models for understanding the cellular effects of stress on cardiac function and metabolism in individuals who have developed cardiac hypertrophy. Hypertrophic cardiac myocytes are forced to change their primary energy source to meet increased demand (Stanley et al. 1997). While the heart normally depends on fatty acid β-oxidation, the hypertrophied heart depends on anaerobic biochemical glycolysis (Sack et al. 1997). A similar metabolic switch happens in the fetus and is governed by a limited oxygen supply in utero versus oxygen abundance available after parturition (Sack et al. 1997). Likewise, enlarged cardiac myocytes cannot obtain adequate oxygen until additional blood vessels develop and supply the heart and, thus, revert to fetal forms of metabolic enzymes that enable glycolysis (Lopaschuk et al. 1991). This makes isolated myocytes from the fetal heart an ideal model for the study of the events involved in stress-induced adult cardiac hypertrophy. We opted for an in vitro approach to studying this phenomenon to isolate cellular events from those which could be influenced by hormonal secretion or widespread events that could occur throughout the circulatory system. The embryonic chick (*Gallus domesticus*) heart served as an ideal source of cardiac cells for a number of reasons: the cells grow readily in culture, their development is under experimental control, and the characteristics of cellular function are similar to those found in mammals (Horres et al. 1987; Ruijtenbeek et al. 2002). In addition, avian models serve as an interesting comparison to mammalian models to uncover universal principles that govern eukaryotic cellular function and regulation.

Materials and Methods

Materials. Unless otherwise indicated, all reagents, chemicals, and antibodies were obtained from Sigma Chemical Co, St. Louis, MO.

Cell cultures. Chick eggs were obtained from a commercial supplier (CBT Farms, Chestertown, MD) and incubated in a forced air incubator at 38°C. Embryonic day 14 chick embryos were removed from the eggs and immediately decapitated. The chest cavities were opened, and hearts (which, at this developmental stage, have fully developed cardiac myocytes; Sedmera et al. 2005) were excised. Hearts were cut into smaller parts and incubated in a centrifuge tube in 0.5% porcine trypsin on ice overnight (Powell and Pitkin 1981). Trypsin was then activated by incubation of the centrifuge tube in a 37°C water bath for 3 min. The tube was vortexed for 2 min followed by vigorous trituration using fire-polished glass pipettes, centrifuged for 5 min, and the pellet was resuspended in culture medium (Iscove's modified Dulbecco's medium+10% fetal bovine serum+1% penicillin/streptomycin). The cell mixture from each heart was distributed to 3 sterile 6-well plates (18 wells in total) containing glass coverslips (22×22 mm, #1 thickness; Thomas Scientific Co., Swedesboro NJ) in 2-ml aliquots. Cell cultures were incubated 2 d in 5% CO_2 at 37°C prior to stress treatments.

Cell treatments. Hyperoxic (HiO) treatments were performed by replacing the culture medium with medium supplemented with 100 μM hydrogen peroxide (Sohal et al. 1989; Schröder and Eaton 2008). Hypoxic (LowO) treatments were performed by removing all culture media and replacing it with deoxy-Ringer's solution (137 mM NaCl, 12 mM KCl, 0.49 mM $MgCl_2$, 0.9 mM $CaCl{\cdot}2H_2O$, 4 mM 4-(2-hydroxyethyl)-1-piperazineethanesulfonic acid [HEPES], 10 mM deoxyglucose, and 20 mM sodium lactate, pH 6.2) sealed in an airtight humidified container, with the air constantly replaced with pure nitrogen. The control, HiO-treated, and LowO-treated plates were then allowed to incubate for 4 h in a 37°C incubator. Culture plates with the control cells were removed from the incubator and handled for an equivalent

amount of time, but did not undergo any other manipulations. Following treatments, cells were returned to the normal culture medium and allowed to grow for an additional time (from 1 through 6 d) prior to testing.

TUNEL staining. Cells were fixed in 4% paraformaldehyde for 10 min. Slides were washed (incubated in phosphate-buffered saline [PBS] for 5 min) thrice and incubated in permeabilization solution (PBS+0.3% Triton X) for 2 min on ice. Positive control cells were incubated with 100 μl DNAse I Recombinant (in 50 mM Tris–HCl, pH 7.5, 10 mg/ml) for 10 min at room temperature. Cells were rinsed twice with PBS, and 50 μl of terminal deoxynucleotidyl transferase dUTP nick end labeling (TUNEL) Reaction Mixture (Roche In Situ Cell Death Detection Kit; Roche Diagnostics Corp., Indianapolis, IN) was added to each coverslip following the manufacturer's instructions. Negative controls were incubated in 50 μl of label solution only. Cells were incubated for 60 min at 37°C in the dark, washed thrice with PBS, mounted on slides with Vectashield (Vector Laboratories, Burlingame, CA), and viewed with a fluorescence microscope and digital camera as described in the succeeding subsections.

Western blotting. Western blots were conducted using standard immunoblotting techniques. Briefly, cells from different treatments were harvested using cell scrapers, lysed, and homogenized in 10 mM Tris buffer in the presence of protease inhibitors, and different cell fractions (nuclei and cytosol) were purified via high-speed centrifugation. Protein concentration was determined using a Coomassie protein assay (Thermo Scientific, Rockford, IL). The fractions were separated on a 15% SDS-polyacrylamide gel using 10 μg protein per lane, transferred to a nitrocellulose membrane, incubated overnight at 4°C with 4% of nonfat dry milk, and reacted with primary antibodies (MyoD=1:500, Santa Cruz Biotech., Santa Cruz, CA; α-sarcomeric actin=1:1,000) for 4 h at room temperature. Uniform gel loading was confirmed using anti-tubulin (for sarcomeric actin or MyoD) or GAPDH (for CaMK) loading control antibodies (Abcam, Cambridge, MA) stained concurrently. Membranes were washed thoroughly in TBST and incubated for 1 h with peroxidase-conjugated secondary antibodies (goat anti-rabbit or anti-mouse polyclonal=1:1,000). Antibody staining was visualized with Pierce ECL Western Blotting Substrate (Thermo Scientific) for 1 min using chemiluminescence, following the manufacturer's instructions.

Immunocytochemistry. Cells were fixed in 4% paraformaldehyde for 10 min and stored in PBS+sodium azide. Cells were washed (incubated in PBS for 5 min) thrice and incubated in blocking solution (PBS+0.3% Triton X+0.1% normal goat serum) for 30 min. Cells were washed thrice in PBS, then incubated overnight in primary antibody (MyoD=1:200, Santa Cruz Biotech., Santa Cruz, CA; α-sarcomeric actin=1:500; CaMKII=1:500) at 4°C. For controls, primary antibodies were substituted with nonimmune serum. Cells were then washed thrice with PBS and incubated in secondary antibody (1:200 goat anti-mouse or anti-rabbit, FITC conjugate for sarcomeric actin and CaMK and TRITC conjugate for MyoD) for 1 h. Cells were washed twice with PBS and twice with deionized water. Slides were stained with 4′,6-diamidino-2-phenylindole (DAPI) for 5 min to visualize nuclei, mounted with Vectashield, and viewed using a fluorescence microscope. Images of cells under transmitted and fluorescence illumination were photographed with ×40 or ×100 objectives using a digital camera attached to the microscope with the exposure set at a constant 1,000 ms.

Images were analyzed using ImageJ (National Institutes of Health, Bethesda, MD). Antibody staining density for sarcomeric actin and CaMK for individual cells was computed from the total area covered by the cell divided by the total area of visible fluorescence staining due to antibody binding, using the threshold functions and algorithms of ImageJ. Since MyoD expression was restricted to the nuclei, MyoD expression was quantified by counting the percentage of nuclei that were MyoD+ versus the total number of nuclei for each treatment (determined using DAPI staining). Data for individual cells or individual trials were averaged, validated with analysis of variance (ANOVA), and compared using Student's t test using a p value of 0.05 to determine significance. Statistical comparisons were made using the Analysis ToolPak of Microsoft Excel.

Calcium imaging. Cells were prepared for imaging as follows: The culture medium in each well was replaced with warm culture medium supplemented with 1 μM Fura-2 and 20 μg/ml pluronic F-127 (Molecular Probes/Invitrogen, Carlsbad, CA). The six-well plates were returned to the incubator for 1 h. Coverslips with Fura-2-loaded cells were then situated in a recording chamber and continuously bathed with a warm Ringer's solution superfusion and secured to the stage of an inverted fluorescence microscope. Cells were visually identified under 360 nm illumination to monitor viability and appropriate Fura-2 loading. Stimulus solutions were applied by switching the superfusion for 10 s; the chamber configuration allowed for a complete exchange of superfusion solutions within 0.5 s while providing a consistent level of fluid over the cells. Cells were constantly superfused with Ringer's solution (145 mM NaCl, 5 mM KCl, 1 mM $CaCl_2$, 1 mM $MgCl_2$, 1 mM Na-pyruvate, and 20 mM HEPES-Na). Cells were stimulated using high-potassium Ringer's solution (Hi K^+; 15 mM NaCl, 135 mM KCl, 1 mM $MgCl_2$, 1 mM Na-pyruvate, 1 mM $CaCl_2$, and 20 mM HEPES-Na), 1 mM epinephrine in Ringer's solution, or 1 mM caffeine in Ringer's solution.

Intracellular calcium concentration ($[Ca^{2+}]_i$) in individual cells was quantified and analyzed as follows: Viable cells

were visually identified under 360 nm excitation. Cells were continuously illuminated at excitation wavelength of 340 nm for 60 s, during which time stimuli were added and removed via superfusion using an automatic high-speed valve. Emitted light from Fura-2 in the cells under ×400 magnification was filtered at 510 nm, integrated over 300 ms, and recorded in "burst mode" with a cooled Hamamatsu Orca CCD camera (12-bit resolution; Hamamatsu Corp., Bridgewater, NJ). Under these conditions, images were acquired every 300 to 305 ms. Image acquisition and analysis was controlled using IPLabs Software (BD Biosciences, Bethesda, MD). This allowed for optimal time resolution of the stimulus-driven $[Ca^{2+}]_i$ changes using our imaging system. Since images were recorded using only one excitation wavelength, the actual values for $[Ca^{2+}]_i$ could not be computed from ratiometric imaging; thus, values for $[Ca^{2+}]_i$ changes are reported as gray levels ranging from 0 to 4,096, with higher values corresponding to higher $[Ca^{2+}]_i$ within the cell. Under these conditions, cells remained viable for several minutes up to 1 h.

Calcium imaging data were analyzed as follows: Individual cells were visually identified and selected by drawing a region of interest (ROI); the software only measured calcium within individual ROIs. Immediately prior to the application of a stimulus solution, the baseline $[Ca^{2+}]_i$ was noted. If a *distinct* and sustained change in $[Ca^{2+}]_i$ following stimulation and a *return* of $[Ca^{2+}]_i$ toward the original baseline following solution removal (within 50 s) were noted, this counted as a response. The response rate was determined by counting the number of cells that responded versus the total number of cells tested; this value was expressed as a percentage±standard error of the mean (SEM) across five replicates (total of 300 cells per treatment). The response time for each individual cell was measured as the time it took for the initial deflection in $[Ca^{2+}]_i$ to occur, up to the time the $[Ca^{2+}]_i$ attained a "steady state" (i.e., no more than two successive increases or decreases in $[Ca^{2+}]_i$ occur). The response duration for each individual cell was determined at the portion of the trace following stimulus removal until the point where the $[Ca^{2+}]_i$ first returned to baseline (at least two or more successive increases or decreases in $[Ca^{2+}]_i$). These measurements were taken for 60 individual cells in each treatment; data are presented as average values±SEM across all cells measured. Average data for individual cells within each treatment were validated with ANOVA and compared against the other treatments with Student's t test using a p value of 0.05 to determine significance. Statistical comparisons were made using the Analysis ToolPak of Microsoft Excel.

Results

For all data, at least five replicates of each experimental run were conducted; data are reported as the average±SEM. Cells were divided into three groups for analysis: control, HiO, and LowO. Cells in the control group were more significantly more abundant (Fig. 1*A*) compared to the HiO and LowO treatment groups. In addition, the control cells grew more quickly and tended to form larger aggregates, whereas cells tended to remain sparser and isolated when treated with LowO or HiO. TUNEL staining was used to quantify dead cells found within each treatment group: the total number of stained nuclei were counted and expressed as a percentage of the total number of cells. The TUNEL staining results (Fig. 1*B*) indicated that, while control cell slides had the greatest percentage of dead cells, this difference was not significant, suggesting that the diminished numbers resulting from the HiO and LowO treatments were likely due to reduced cell proliferation and/or increased cell differentiation rather than increased cell death.

Structural attributes. Immunocytochemistry was performed on days 3 and 8 after cell cultures were established (1 or 6 d after stress treatment) to quantify short-term and long-term structural reorganization occurring as a result of treatment conditions. Differentiated myocytes were identified using α-sarcomeric actin; levels of this protein were measured using immunocytochemistry and Western blotting, as described in

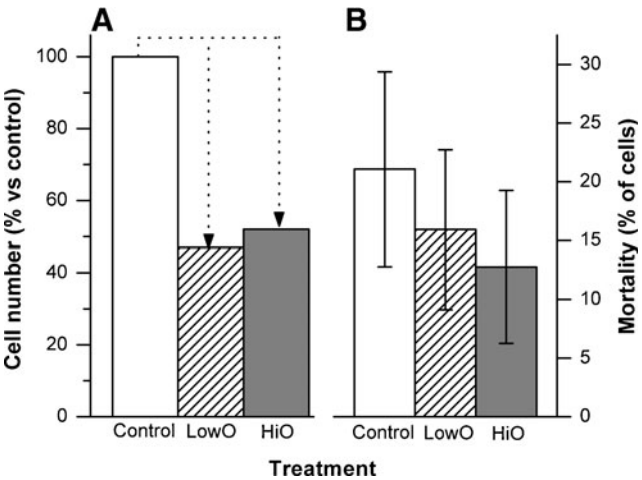

Figure 1. Hypoxic and hyperoxic treatments do not affect apoptosis. Cardiac myocytes were grown in culture using standard methods. HiO and LowO treatments were performed, as described in the "Materials and Methods" section. (*A*) After 8 d, the total number of cells on each coverslip was counted using DAPI staining to visualize nuclei; cells were fixed and TUNEL staining was performed, as described in the "Materials and Methods" section. The total number of cells in each six-well plate from the same batch was counted and expressed as a percentage relative to the controls. In this and in subsequent figures, *dotted lines* indicate a significant difference between treatments (in this case, both LowO and HiO were significantly different from the controls). (*B*) The proportion of dead cells (determined by TUNEL staining) expressed as a percentage of stained nuclei over the total number of cells. There is a greater mortality in the control group (although the difference is not statistically significant), indicating that the differences in cell density resulting from HiO and LowO treatments were due to downregulated division/proliferation rather than increased cell death. The data were averaged from five separate runs of the experiment.

the "Materials and Methods" section. Data presented were averaged from five replicates of the experiment, measured from a total of 80 cells per treatment. Sarcomeric actin in cells at early stages of differentiation appeared as diffuse, non-discrete staining found throughout the cell, appearing denser adjacent the nucleus and at the periphery of the cell (Fig 2*A*, *B*). As cells proceeded through differentiation, striations and thick polymerized filaments were visually evident (as in Fig. 2*C*, *D*). In both LowO (Fig. 2*C*) and HiO (Fig. 2*D*) treatment groups, overall sarcomeric actin expression was denser and showed more polymerization and striation than in the control cells (Fig. 2*B*) on day 3. By day 8, majority of the cells across all treatments showed similar sarcomeric actin staining patterns (similar to Fig. 2*C*, *D*). We quantified sarcomeric actin using Western blotting (Fig. 2*E*) and immunostaining (Fig. 2*F*), as described in the "Materials and Methods" section; these measures confirmed the visual observations: sarcomeric actin was significantly greater in LowO and HiO treatments at day 3, and by day 8, this difference was no longer present, mainly due to the fact that control cells eventually upregulated actin expression (Fig. 2*E*, *F*). These changes indicate that hyperoxic stress resulted in an upregulation and reorganization of structural proteins (indicative of hypertrophy) within a short time window.

To initiate muscle differentiation, MyoD is expressed in the myocyte nucleus early in differentiation; its expression declines over time as cells continue to differentiate (Van Bilsen and Chien 1993). We immunostained cells from the different treatment groups for MyoD (Fig. 3*A–C*). As expected, MyoD staining was localized to the nucleus. From visual inspection, it appeared that, at day 3, more cells in the HiO treatment (Fig. 3*C*) expressed MyoD when compared to the controls (Fig. 3*A*) or the LowO treatment (Fig. 3*B*). In addition, MyoD did not co-localize with sarcomeric actin (Fig. 3*D*), supporting the notion that MyoD is expressed early in the differentiation process prior to the synthesis of sarcomeric actin. We quantified MyoD, as described in the "Materials and Methods" section; data were averaged from cell counts across five individual trials. In both our LowO and HiO treatment groups at day 3, MyoD production was higher (Fig. 3*E*) and was present in a significantly larger number of cells (Fig. 3*F*) compared to the controls. These results supported the data seen in Fig. 2 since the production of MyoD is indirectly related to sarcomeric actin production (Olson 1993). Interestingly, cells exposed to HiO appeared to terminally differentiate: no new

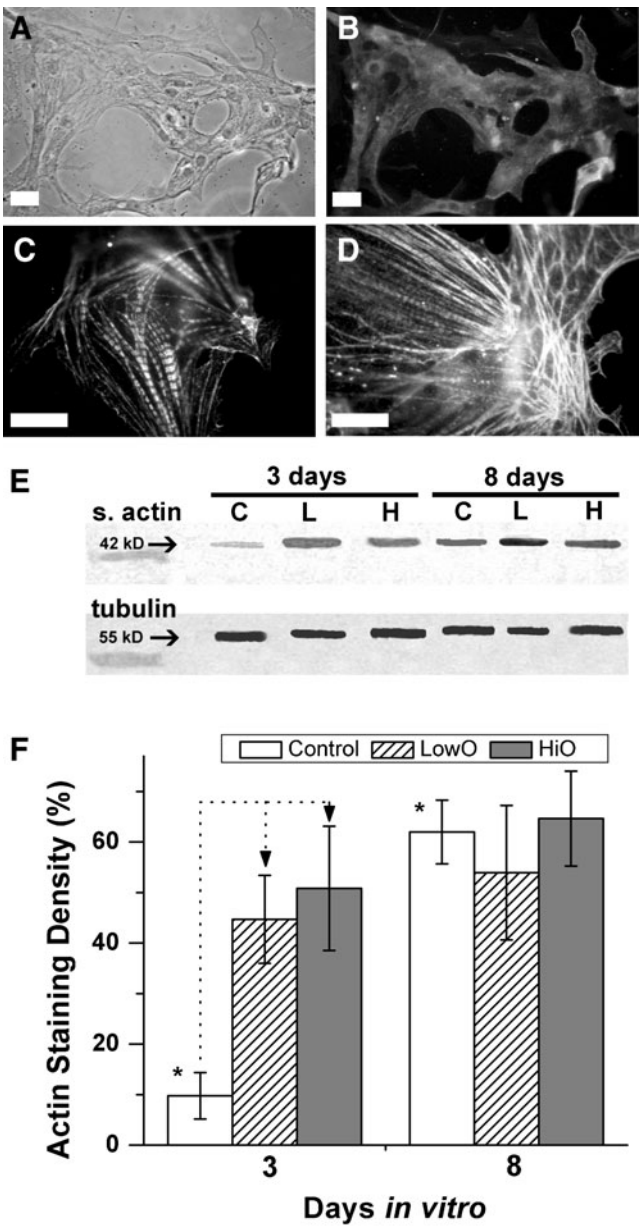

Figure 2. Both hypoxia and hyperoxia induce an upregulation in sarcomeric actin expression. (*A*) Phase contrast photomicrograph of control cells taken at day 3 shows a cluster of cardiac myocytes; a variety of cell types was typically seen in vitro. *Scale bar* for this and all subsequent figures=20 μm. (*B*) Actin immunostaining of the cells shown in *A*. In these cells, sarcomeric actin was expressed at much lower levels, with few cells showing discrete polymerization. (*C*) Immunofluorescence photomicrograph of LowO-treated cells shows sarcomeric actin polymerized into discrete filaments. (*D*) HiO-treated cells had very dense sarcomeric actin filaments with more extensive polymerization. Cells in the different treatments at day 8 all showed a similar staining pattern as the one shown in this image. (*E*) Western blots showing sarcomeric actin and tubulin (as a loading control). Sarcomeric actin levels are markedly reduced with day 3 controls, but show similar density levels for all other treatments. (*F*) Sarcomeric actin staining density for control, LowO-treated, and HiO-treated cells at days 3 and 8 were measured in individual cells and averaged. At day 3, both LowO and HiO treatments resulted in a significantly increased amount of actin expression; this difference was not present at day 8. At day 3, actin expression in LowO-treated and HiO-treated cells reached a level that did not increase any further as time progressed. For this and subsequent figures, symbols (*asterisks*, *plus signs*) indicate significant differences that emerge over time within the same treatment (in this case, a significant difference between the controls at day 3 versus 8). Data presented were averaged from five replicates of the experiment, measured from a total of 80 cells per treatment.

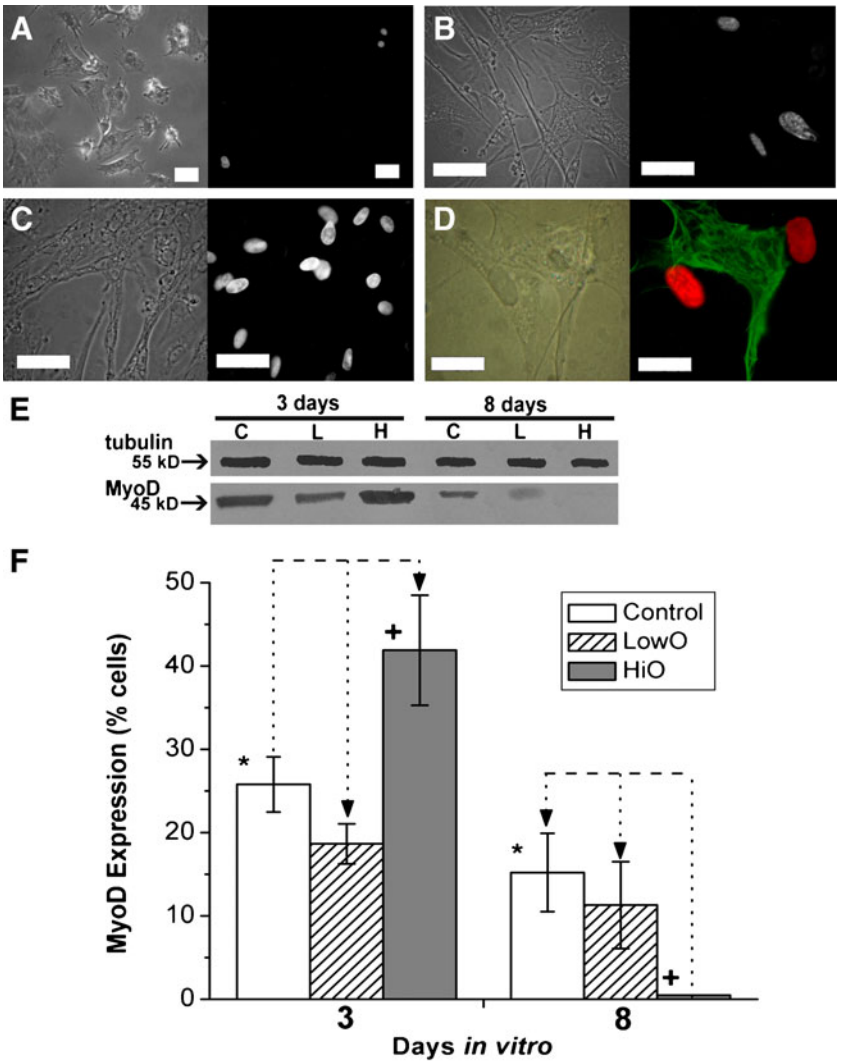

Figure 3. Effects of hypoxia and hyperoxia on MyoD expression. Cardiac myocytes were grown in culture and immunostained, as described in the "Materials and Methods" section; staining was visualized under a TRITC filter. MyoD staining, which was expectedly localized to the nucleus, was quantified by counting the number of stained nuclei versus the total number of cells. For all images, *scale bar* = 20 μm. Phase contrast image (*left panel*) and the corresponding immunofluorescence image (*right panel*) show that few cells in the controls (*A*) or LowO treatments (*B*) expressed MyoD. (*C*) HiO treatment resulted in a significantly increased amount of MyoD expression. (*D*) Phase contrast image (*left panel*) and the corresponding composite immunofluorescence image (*right panel*) of double labeling of sarcomeric actin (*green*) and MyoD (*red*) show that these two proteins did not co-localize to the same cells. (*E*) Western blots of MyoD from the different treatments show the changes in MyoD expression due to the different treatments over time. At day 3, the MyoD band appears less intense in the LowO treatment and more intense in HiO treatments compared to the controls. At day 8, no MyoD expression was seen in the HiO-treated cells, indicating that all cells had completely differentiated at this point, while controls and LowO treatment batches still showed some MyoD expression. (*F*) MyoD expression was determined, as described in the "Materials and Methods" section. At day 3, both LowO and HiO expression were significantly different from the controls. At day 8, MyoD showed an overall reduction in expression and was completely absent in HiO-treated cells. Data are presented as an average of six replicates of the experiment (300 cells per treatment).

MyoD expression was seen at day 8, while cells in the controls and LowO treatment continued to express MyoD (Fig. 3*E*, *F*). Over time through day 8, controls and HiO-treated cells significantly decreased their MyoD expression, while the cells in the LowO treatment appeared to continue to maintain MyoD expression.

CaMK staining in control cells was regularly dispersed throughout the cytosol, increasing in density near the nucleus (Fig. 4*A*). At day 3, LowO (Fig. 4*B*) but not HiO treatment (Fig. 4*C*) resulted in a visibly decreased CaMK expression. By day 8, CaMK expression appeared to be identical through the different treatment groups: Fig. 4*D* shows the staining pattern in control cells from day 8 that is representative across all treatments. When protein levels were measured using Western blotting (Fig. 4*E*) or immunostaining (Fig. 4*F*; data averaged from 40 cells per treatment), it showed that CaMK expression at day 3 was reduced by LowO but not HiO treatment. At day 8, this trend appeared to hold, but the data

were no longer statistically significant: CaMK staining density was not significantly different in LowO-treated versus HiO-treated cells, nor did it show a significant change from days 3 to 8. Thus, while both HiO and LowO treatments resulted in structural changes, LowO treatment resulted in a reduction in the CaMK protein that is critical for myocyte function.

Functional attributes. The calcium imaging provided a detailed measure of the differences in functional changes in cardiac myocytes exposed to HiO and LowO conditions. Stimulation would expectedly trigger a $[Ca^{2+}]_i$ response in intact cells, as the signaling pathways triggered by potassium, caffeine, or epinephrine ultimately resulted in calcium release by the sarcoplasmic reticulum for the initiation of myosin contraction (Sitsapesan and Williams 1990). For simplicity, we only show data measured from the cells 3 d posttreatment (60 cells per treatment); extended time in culture did not result in a significant difference in the functional properties between the different treatments (data not shown).

Changes in $[Ca^{2+}]_i$ occurring after stimulation result from signal cascades that open channels in the sarcoplasmic reticulum and allow calcium to passively diffuse into the cytosol. This change in $[Ca^{2+}]_i$ constituted the rise time as measured by this study (Fig. 5*A*, *a* to *b*). After release and the subsequent muscle activity, $[Ca^{2+}]_i$ is actively transported back into the sarcoplasmic reticulum, returning $[Ca^{2+}]_i$ to baseline. Because of the time requirements of active transport, it was expected that the response duration (Fig. 5*A*, *b* to *c*) would be much longer than the stimulus application and that recovery times (Fig. 5*A*, *c* to *d*) would be much longer than the rise times. For simplicity, since we found that recovery time was correlated with response duration (data not shown), we did not report these values. Since we did not do ratiometric calcium imaging measurements, we could not measure (and, thus, compare) the magnitude of the $[Ca^{2+}]_i$ change across the different treatments.

Responses to K^+ depolarization (Hi K^+; Fig. 5*B*) would not involve signaling pathways. Thus, these $[Ca^{2+}]_i$ fluxes typically had a faster rise time and recovery time and a shorter duration compared to responses to pharmacological stimuli.

When challenged with epinephrine or caffeine, the response properties of the HiO-treated versus LowO-treated cells differed. The response rates for cells treated with LowO or HiO was generally higher compared to the controls, most likely due to the lower overall number and increased differentiation rates elicited by these treatments. A closer examination of the kinetic properties shows differences elicited by the treatments: when stimulated with caffeine or epinephrine, treatment with HiO resulted in a $[Ca^{2+}]_i$ response wherein the rise time was significantly longer than control cells or those treated with LowO. In contrast, treatment with LowO resulted in a caffeine-elicited $[Ca^{2+}]_i$ response with a significantly shorter rise time compared to HiO-treated cells and a significantly longer rise time compared to the controls.

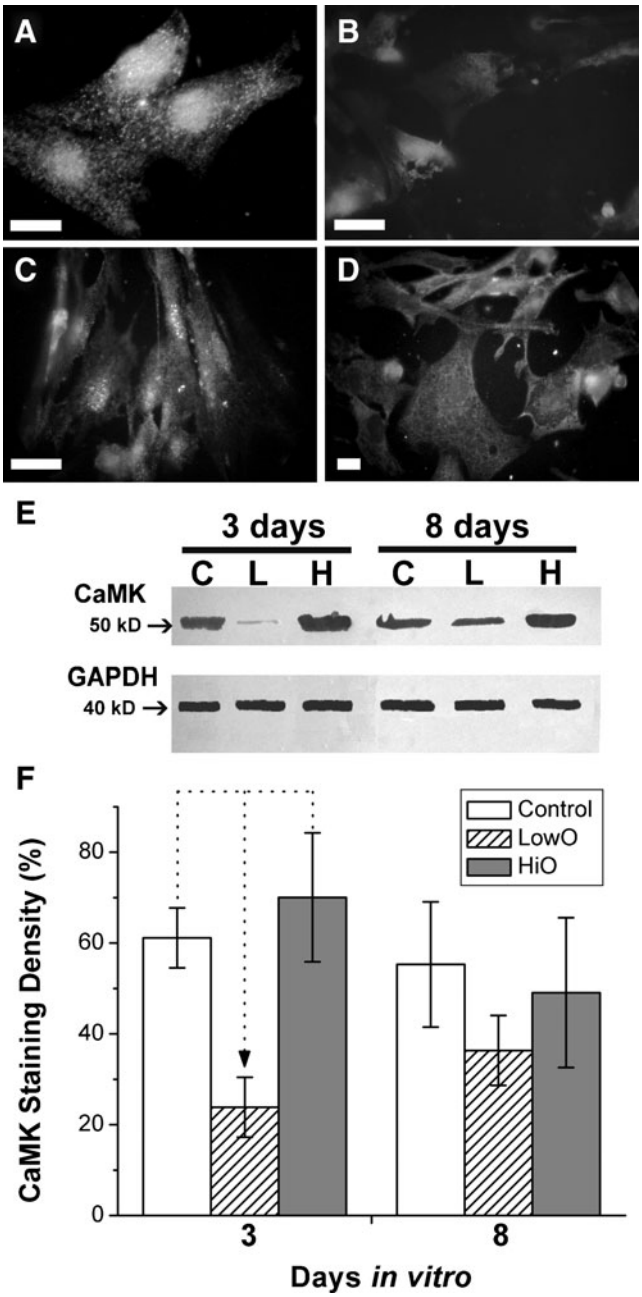

Figure 4. CaMK expression is differentially affected by hypoxia and hyperoxia. (*A*) Sample image of CaMK immunostaining in control cells shows that CaMK is distributed throughout the cytosol. For all images, *scale bar*=20 μm. CaMK expression was markedly reduced in LowO-treated cells (*B*) but not in HiO-treated cells (*C*). (*D*) CaMK staining in control cells (shown) or in either LowO-treated or HiO-treated cells was similar to the pattern seen in day 3. (*E*) Western blots of CaMK show that only the LowO treatment at day 3 showed a marked difference from any of the other treatments. (*F*) The immunostaining density was measured for each cell after 3 or 8 d, as described in the "Materials and Methods" section, and averages were calculated. At day 3, LowO treatment resulted in significantly lower amounts and HiO treatment resulted in a significantly increased CaMK expression compared to controls; CaMK staining density was not significantly different in LowO-treated versus HiO-treated cells, nor did they significantly change from days 3 to 8. Data are presented as an average of four replicates of the experiment, measured from 40 cells per treatment.

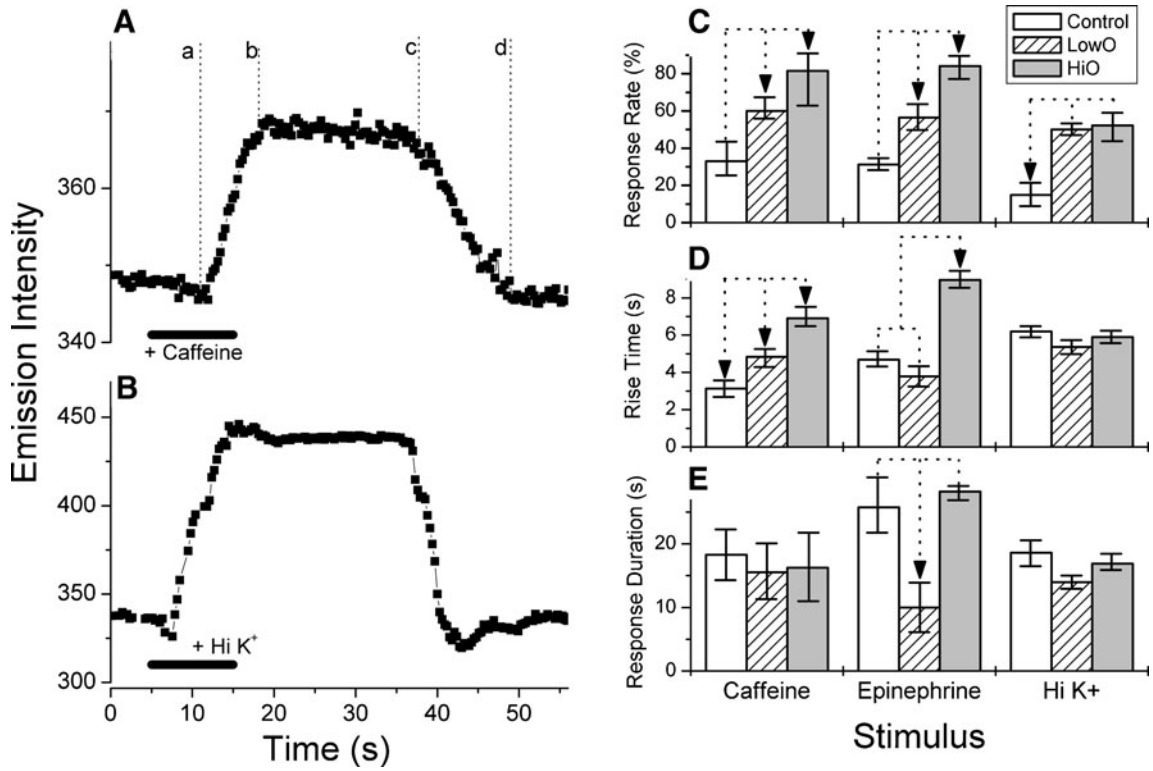

Figure 5 Calcium imaging data show a difference in functional properties resulting from LowO and HiO treatments. (*A*) Sample data traces from $[Ca^{2+}]_i$ imaging studies: stimuli were bath-applied for 10 s with either caffeine, epinephrine, or Hi K^+ (*solid bars*), as described in the "Materials and Methods" section. Cell responses were typically prolonged and outlasted the stimulus application by several seconds. To quantify cell responses, we measured the rise time (from *a* to *b*) and the duration (from the end of stimulus application to *c*); recovery time (from *c* to *d*) was correlated to duration and, thus, not reported. (*B*) A sample data trace from a cell that responded to Hi K^+. Responses to K^+ depolarization typically had a faster rise time and recovery time and a shorter duration compared to pharmacological stimuli. In general, cell responses to Hi K^+ were not significantly affected by different oxidative stress treatments. (*C*) Response rates of cells under the different treatments were measured, as described in the "Materials and Methods" section. Note that, since the overall cell numbers for both LowO-treated and HiO-treated cells was lower, the response rates for these cells was generally higher. (*D*, *E*) Treatment with HiO resulted in a $[Ca^{2+}]_i$ response wherein the rise time and duration were significantly longer when stimulated with caffeine or epinephrine. In contrast, treatment with LowO resulted in a $[Ca^{2+}]_i$ response with a significantly shorter rise time and duration. (*C–E*) *Dotted lines* and *arrowheads* indicate a significant difference between the different treatments. Data for each *bar* are presented as an average of five replicates of the experiment (measured from 60 cells total).

When stimulated with epinephrine, these cells had a significantly shorter rise time and response duration compared to HiO-treated cells.

Treatment with LowO or HiO resulted in a significantly increased proportion of cells that responded to Hi K^+ (Fig. 5*C*). These results support the data previously described: oxidative stress treatment results in increased rates of cell differentiation and hypertrophy. The kinetic properties (rise time and response duration) of cell responses to Hi K^+ (Fig. 5*D*, *E*), however, were not significantly affected by different oxidative stress treatments.

In summary, both LowO and HiO treatment results in an overall reduction in cell numbers and an increased rate of cell differentiation and hypertrophy within 3 d of treatment. However, the cellular mechanisms that regulate contractile activity appear to be differentially affected by LowO and HiO treatment: the stimulus-elicited $[Ca^{2+}]_i$ response is augmented by HiO treatment and suppressed by LowO treatment; these effects are specific to pathways mediated by signaling pathways. These results suggest that the structural hypertrophy that is elicited by these two different treatments may differ primarily in the functional properties of stimulus-elicited $[Ca^{2+}]_i$ fluxes mediated by cell signaling pathways.

Discussion

This study demonstrates that, while hypoxic (pathological) and hyperoxic (physiological) factors both induce similar structural changes in hypertrophied cardiac myocytes, they can cause differential functional changes at the subcellular level, particularly in terms of ligand-based signaling pathways. Treated cells exhibit significantly different response times when stimulated with epinephrine, indicating that the signaling cascades resulting from activated β-adrenergic

receptors, which regulate various other cellular functions, may have been compromised (Ventura et al. 1992). The in vitro approach allowed us to demonstrate that this effect is exerted at the single-cell level, separate from the influence of hormonal fluxes in the whole organism, or syncytial behavior that is present in an intact organ. Because of the widespread effects each of the second messenger proteins can have on other cellular functions and the degree of cross-signaling present, it is likely that hypertrophied cardiac myocytes can exhibit functional changes not observed in this study (Hefti et al. 1997). Furthermore, the conditions in our preparation are radically different from conditions in situ: the cells were typically isolated and were not syncytial, and the growth factors usually present in the whole embryo were not added.

These results indicate that production of α-sarcomeric actin and the transcription factor MyoD are both upregulated during hypertrophy resulting from hypoxic and hyperoxic conditions. Previous studies have shown that that hypoxidative or hyperoxidative stress causes compensatory organizational changes in nearly all cell organelles (Dhalla et al. 2009), suggesting that cardiac hypertrophy is dependent upon genetic control. However, the diversity of signals that trigger hypertrophy can affect many different pathways that cooperate to produce a variety of different transcription factors. The transcribed proteins ultimately produce the structural reorganization exhibited by the cells exposed to HiO and LowO conditions on day 3 as an upregulation of sarcomeric actin (Hefti et al. 1997). These changes in structural reorganization were significantly affected on day 3 but not on day 8, suggesting that the hypertrophic changes in cardiac myocytes are acute changes, and manifested primarily within a brief critical time window.

CaMK phosphorylation controls the activation of sarcomeric myosin filaments during muscle contraction. Therefore, it is expected that an upregulation of contractile proteins as a compensatory mechanism during cardiac hypertrophy would also result in an upregulation of the proteins that control their activation. This accounts for the changes seen in Fig. 3, wherein CaMK expression increased in both LowO-treated and HiO-treated cells at day 3.

The results of calcium imaging indicated that hypoxic or hyperoxic stress initiate different functional changes in cardiac myocytes that occur when cells are stimulated with caffeine and epinephrine (Molkentin 2006). Caffeine and epinephrine act on cardiac myocytes using similar, albeit crossed, signaling pathways that are initiated at the β-adrenergic receptor located on the myocyte cell membrane and have been shown to increase intracellular $[Ca^{2+}]_i$ in hypertrophied cardiac myocytes (Ventura et al. 1992; Hefti et al. 1997). $[Ca^{2+}]_i$ changes that occur in cardiac myocytes are typically prolonged due to simultaneous calcium release and uptake by the sarcoplasmic reticulum (Bassani et al. 1992). Studies showed that caffeine-activated $[Ca^{2+}]_i$ release from the sarcoplasmic reticulum of cardiac myocytes was counteracted by activation of the sodium–calcium exchanger, which pumps calcium out of the cell, further prolonging the calcium response that governs muscle contraction (Callewaert et al. 1989). Additionally, calcium buffers and protein phosphorylation contribute to the length of $[Ca^{2+}]_i$ stabilization during calcium imaging (Maier and Bers 2007).

Calcium imaging data for cells under Hi K^+ stimulation indicated that the observed differences in functional changes within the heart did not occur as a result of changes in the voltage-gated channels governing cell depolarization or from changes in CaMK production. Additionally, CaMK was present in a quantity that was adequate enough to regulate contraction, further indicating that this protein is not involved in a pathological response to hypertrophy (Maier and Bers 2007). Thus, the observed differences were most likely due to elements of receptor-mediated signaling.

In HiO-treated cells, the caffeine-stimulated $[Ca^{2+}]_i$ response and recovery were more robust (slower rise time and longer response duration) than the controls, while in the LowO-treated cells, the epinephrine-stimulated $[Ca^{2+}]_i$ response was significantly weaker (more transient) than the controls (Fig. 5*E*). Since epinephrine and caffeine both initiate ligand-activated signaling cascades in cardiac myocytes, these results indicate that these pathways are differentially affected by pathologic and physiologic hypertrophy. It is likely that the changes in transcription regulation (Fig. 3) may simultaneously affect components of signaling cascades. Additionally, these results demonstrate the extensive cross-signaling and diverse cellular responses that may occur in response to stimulation of a single receptor type. What is most curious is that these changes occur in isolated cells, suggesting that mechanisms for sensing and responding to hypoxic and hyperoxic conditions are present at the cellular level via mechanisms such as redox switches (Palumaa 2009). This clearly merits further investigation.

In summary, the results of our study suggest that the differences in cardiac myocyte hypertrophy induced by physiological or pathological conditions lie mainly in the functional attributes. The structural rearrangement occurring in the contractile protein upregulation during hypertrophy is not in itself detrimental. Similarly, voltage-gated channels and the regulation of myosin activation by CaMK are unchanged by hyperoxic or hypoxic conditions. However, the changes in transcriptional regulation that cause these structural changes may also affect components of ligand-activated signaling pathways, which are likely initiated and regulated at the cellular level. Although this study does not specifically address whether the observed changes to signaling cascades or calcium stores are beneficial or detrimental, it suggests that changes in these pathways may be responsible for the detrimental outcomes associated with pathologically induced hypertrophy on an organismal level.

Acknowledgment This work was partially supported by funds from the University of Scranton Presidential Fellowship for Summer Research to AG.

References

Aoki H.; Sadoshima J.; Izumo S. Myosin light chain kinase mediates sarcomere organization during cardiac hypertrophy in vitro. *Nat. Med.* 6: 183–188; 2000.

Bassani R. A.; Bassani J. W. M.; Bers D. M. Mitochondrial and sarcolemmal Ca^{2+} transport reduce $[Ca^{2+}]_i$ during caffeine contractures in rabbit cardiac myocytes. *J. Physiol.* 453: 591–608; 1992.

Berlin J. R.; Konishi M. Ca^{2+} transients in cardiac myocytes measured with high and low affinity Ca^{2+} indicators. *Biophys. J.* 65: 1632–1647; 1993.

Bers D. M. Calcium fluxes involved in control of cardiac myocyte contraction. *Circ. Res.* 87: 275–281; 2000.

Callewaert G.; Cleemann L.; Morad M. Caffeine-induced Ca^{2+} release activates Ca^{2+} extrusion via Na^{+}–Ca^{2+} exchanger in cardiac myocytes. *Am. J. Physiol.* 257: C147–C152; 1989.

Chien K. R.; Zhu H.; Knowlton K. U.; Miller-Hance W.; Van-Bilsen M.; O'Brien T. X.; Evans S. M. Transcriptional regulation during cardiac growth and development. *Annu. Rev. Physiol.* 55: 77–95; 1993.

Dhalla N. S.; Saini-Chohan H. K.; Rodriguez-Leyva D.; Elimban V.; Dent M. R.; Tappia P. S. Subcellular remodeling may induce cardiac dysfunction in congestive heart failure. *Cardiovasc. Res.* 81: 429–438; 2009.

Frey N.; Olson E. N. Cardiac hypertrophy: the good, the bad, and the ugly. *Annu. Rev. Physiol.* 65: 45–79; 2003.

Gaasch W. H.; Zile M. R.; Hoshino P. K.; Weinberg E. O.; Rhodes D. R.; Apstein C. S. Tolerance of the hypertrophic heart to ischemia. Studies in compensated and failing dog hearts with pressure overload hypertrophy. *Circulation* 81: 1644–1653; 1990.

Hefti M. A.; Harder B. A.; Eppenberger H. M.; Schaub M. C. Signaling pathways in cardiac myocyte hypertrophy. *J. Mol. Cell. Cardiol.* 29: 2873–2892; 1997.

Horres C. R.; Wheeler D. M.; Piwnica-Worms D.; Lieberman M. Ion transport in cultured heart cells. In: Pinson A. (ed) The heart cell in culture. CRC, Boca Raton, pp 77–108; 1987.

Kong S. W.; Bodyak N.; Yue P.; Liu Z.; Brown J.; Izumo S.; Kang P. M. Genetic expression profiles during physiological and pathological cardiac hypertrophy and heart failure in rats. *Physiol. Genomics* 21: 34–42; 2005.

Lopaschuk G. D.; Spafford M. A.; Marsh D. R. Glycolysis is predominant source of myocardial ATP production immediately after birth. *Am. J. Physiol.* 261: H1698–H1705; 1991.

Maier L. S.; Bers D. M. Role of Ca^{2+}/calmodulin-dependent protein kinase (CaMK) in excitation–contraction coupling in the heart. *Cardiovasc. Res.* 73: 631–640; 2007.

Molkentin J. D. Dichotomy of Ca^{2+} in the heart: contraction versus intracellular signaling. *J. Clin. Invest.* 116: 623–626; 2006.

Moore R. L.; Korzick D. H. Cellular adaptations of the myocardium to chronic exercise. *Prog. Cardiovasc. Dis.* 37: 371–396; 1995.

Olson E. N. Regulation of muscle transcription by the MyoD family. The heart of the matter. *Circ. Res.* 72: 1–6; 1993.

Palumaa P. Biological redox switches. *Antioxid. Redox Signal.* 11: 981–983; 2009.

Powell J. A.; Pitkin R. B. Laboratory on organ culture of chick heart embryos. *Am. Biol. Teach.* 43: 43–44; 1981.

Richey P. A.; Brown S. P. Pathological versus physiological left ventricular hypertrophy: a review. *J. Sports Sci.* 16: 129–141; 1998.

Ruijtenbeek K.; De Mey J. G.; Blanco C. E. The chicken embryo in developmental physiology of the cardiovascular system: a traditional model with new possibilities. *Am. J. Physiol. Regul. Integr. Comp. Physiol.* 283: R549–R551; 2002.

Sack M. N.; Disch D. L.; Rockman H. A.; Kelly D. P. A role for Sp and nuclear receptor transcription factors in a cardiac hypertrophic growth program. *Proc. Natl. Acad. Sci. U. S. A.* 94: 6438–6443; 1997.

Sassoon D. A.; Garner I.; Buckingham M. Transcripts of α-cardiac and α-skeletal actins are early markers for myogenesis in the mouse embryo. *Development* 104: 155–164; 1988.

Schröder E.; Eaton P. Hydrogen peroxide as an endogenous mediator and exogenous tool in cardiovascular research: issues and considerations. *Curr. Opin. Pharmacol.* 8: 153–159; 2008.

Sedmera D.; Reckova M.; Rosengarten C.; Torres M. I.; Gourdie R. G.; Thompson R. P. Optical mapping of electrical activation in the developing heart. *Microsc. Microanal.* 11(3): 209–215; 2005.

Sitsapesan R.; Williams A. J. Mechanisms of caffeine activation of single calcium-release channels of sheep cardiac sarcoplasmic reticulum. *J. Physiol.* 423: 425–439; 1990.

Sohal R. S.; Marzabadi M. R.; Galaris D.; Brunk U. T. Effect of ambient oxygen concentration on lipofuscin accumulation in cultured rat heart myocytes—a novel in vitro model of lipofuscinogenesis. *Free Radic. Biol. Med.* 6: 23–30; 1989.

Song L. S.; Wang S. Q.; Xiao R. P.; Spurgeon H.; Lakatta E. G.; Cheng H. β-Adrenergic stimulation synchronizes intracellular Ca^{2+} release during excitation–contraction coupling in cardiac myocytes. *Circ. Res.* 88: 794–801; 2001.

Stanley W. C.; Lopaschuk G. D.; Hall J. L.; McCormack J. G. Regulation of myocardial carbohydrate metabolism under normal and ischaemic conditions. Potential for pharmacological interventions. *Cardiovasc. Res.* 33: 243–257; 1997.

Van Bilsen M.; Chien K. R. Growth and hypertrophy of the heart: towards an understanding of cardiac specific and inducible gene expression. *Cardiovasc. Res.* 27: 1140–1149; 1993.

Ventura C.; Spurgeon H.; Lakatta E. G.; Guarnieri C.; Capogrossi M. C. Kappa and delta opioid receptor stimulation affects cardiac myocyte function and Ca^{2+} release from an intracellular pool in myocytes and neurons. *Circ. Res.* 70: 66–81; 1992.

Waypa G. B.; Marks J. D.; Mack M. M.; Boriboun C.; Mungai P. T.; Schumacker P. T. Mitochondrial reactive oxygen species trigger calcium increased during hypoxia in pulmonary arterial myocytes. *Circ. Res.* 91: 719–726; 2002.

Zhang T.; Maier L. S.; Dalton N. D.; Miyamoto S.; Ross J.; Bers D. M.; Brown J. H. The δC isoform of CaMKII is activated in cardiac hypertrophy and induces dilated cardiomyopathy and heart failure. *Circ. Res.* 92: 912–919; 2003.